Development of an electrochemical biosensor for the detection of mammary gland carcinoma using molybdenum enhanced poly taurine nano-biofilms confirmed pathological findings

Hassan Nasrollahpour[1], Balal Khalilzadeh[2*] ◉, Reza Rahbarghazi[2,3], Nevin Erk[4], Mohammad-Reza Rashidi[5] and Abdolhossein Naseri[1*]

*Correspondence:
khalilzadehb@tbzmed.ac.ir;
balalkhalilzadeh@gmail.com;
a_naseri@tabrizu.ac.ir

[1] Department of Analytical Chemistry, Faculty of Chemistry, University of Tabriz, 51644-14766, Tabriz, Iran
[2] Stem Cell Research Center, Tabriz University of Medical Sciences, 51644-14766, Tabriz, Iran
[3] Department of Applied Cell Sciences, Faculty of Advanced Medical Sciences, Tabriz University of Medical Sciences, Tabriz, Iran
[4] Department of Analytical Chemistry, Faculty of Pharmacy, Ankara University, 06560 Ankara, Turkey
[5] Department of Medicinal Chemistry, Faculty of Pharmacy, Tabriz University of Medical Sciences, Tabriz, Iran

Abstract

Background: Developing high-performance sensing frameworks for diagnosing anaplastic changes is the subject of debate. The lack of on-time diagnosis in patients with suspicious cancers can affect the prognosis and survival rate. As a correlate, the emergence of de novo strategies for developing transducing frameworks has an inevitable role in advanced biosensing. The combination of green chemistry procedures with eco-friendly and biocompatible materials is of high desirability in this context. The synthesis of new biocompatible and cost-effective nanomaterials to meet the emerging needs of rising demands appeals to new synthetic methodologies.
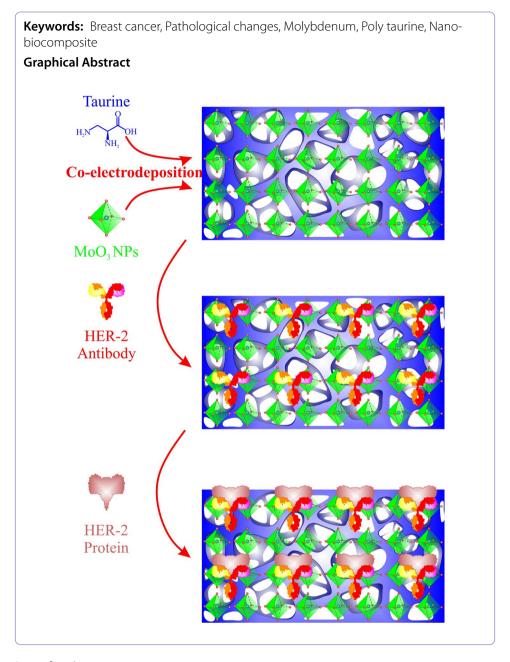
Methods: Here, we applied the electrochemical synthesis method to the fabrication of biocompatible and subtly governed Molybdenum trioxide/poly taurine nano-bio films to monitor human epidermal growth factor receptor-2 (HER-2) in sera from breast cancer patients. Morphological and elemental assessments were performed using a scanning electron microscope, energy-dispersive X-Ray spectroscopy, and dot mapping analyses. In addition, HER-2 immunohistochemistry (IHC) staining was performed on tissue samples, and data were compared to the values obtained by Molybdenum trioxide/poly taurine nano-bio films.

Results: We also noted our platform is eligible for feasible, rapid, and specific determination of HER-2 factor in human samples. The method had a lower limit of quantification of 0.000001 ng/mL and a linear dynamic range between 0.1 ng/mL and 0.000001 ng/mL. IHC imaging showed that the degree of anaplastic changes in breast samples (intensity of HER-2 factor) was closely associated with the intensity of signals obtained by our developed immunosensor.

Conclusions: According to the obtained desirable coordination with pathological studies, the designed biosensor has excellent capability to use as a reliable diagnostic tool in clinical laboratories.

Graphical Abstract

Introduction

Breast cancer (BC) is one of the most devastating malignancies and the second-leading mortality cause in females worldwide. Traditional methods for BC screening include magnetic resonance imaging (MRI), ultrasound, mammography, or positron emission tomography (PET scans). Unfortunately, these approaches possess several drawbacks, such as high cost, low sensitivity, invasiveness, and difficult operation with stressful conditions for patients (Kim et al. 2020; Loyez et al. 2020). Several BC biomarkers, such as nucleotides, cancer cells, proteins, and some small molecules, have been explored to support a more precise and convenient diagnosis than conventional methods. Of these biomarkers, the human epidermal growth factor receptor-2 (HER-2), a specific onco-protein, is changed during the development and progression of BC (Nasrollahpour

et al. 2021a). It was suggested that the overexpression of HER-2 in breast cancer cells stimulates proliferation rate and tumor expansion (Chen et al. 2019; Sharma et al. 2018). Currently, the biomarker assisted diagnosis of HER-2$^+$ BC is based on conventional techniques like cytological analyses using fine-needle aspiration (FNA), fluorescence in situ hybridization (FISH), gene expression monitoring, immunohistochemistry (IHC), and enzyme-linked immunosorbent assay (ELISA) procedures. Among the above-mentioned approaches, FNA and direct sampling are time-consuming and operationally invasive and can result in iatrogenic tumor implantation or metastasis (Tabasi et al. 2017). Importantly, laboratory data have indicated that the level of HER-2 in the serum of BC patients ranged from 220 pM to 1.1 nM whereas these values reached 30 pM to 220 pM in healthy people, showing the much overlaps in the systemic levels of HER-2 under physiological and pathological conditions (Ranganathan et al. 2020; Chun et al. 2013; Shen et al. 2018). Consequently, there is an urgent need to develop more accurate and low-cost methodologies with the ability for rapid and sensitive recognition in BC patients.

Biosensors have been developed as key responses to circumvent the problems associated with HER-2 screening (Karimzadeh et al. 2020; Pourakbari et al. 2019). Electrochemical biosensors are one of the most employed, highly sensitive, and easily implemented tools for detecting target molecules in biological samples (Cesewski and Johnson 2020; Wang et al. 2017; Min et al. 2021; Khalilzadeh et al. 2019; Mansouri et al. 2020). One of the most appealing interests in electrochemical biosensing strategies is using nano-biomaterials to modify electrode surface structure (Chenaghlou et al. 2021; Isildak et al. 2020). The simultaneous application of nanomaterials in electrochemical sensors can yield excellent achievements (Zhang and Chen 2019; Wongkaew et al. 2018; Gupta et al. 2021). The synthesis protocol of nanomaterials is one of the limiting factors in their applicability, quality, final costs, and environmental viewpoints (Chen et al. 2018; Kolahalam et al. 2019). Thanksgiving to colloidal procedures, electrosynthesis of nanomaterials is easily performed by dipping the working electrode in the electrochemical cell containing the precursor solution. A load of the same nanostructures on working electrodes using electrochemical methods is thought to increase detection outcomes (Wang et al. 2020; Ansari et al. 2020; Zhang et al. 2020; Nasrollahpour et al. 2021b). In this case, there are no reducing or stabilizing agents in the growth solution, which were applied in colloidal methodologies. Instead, a specified potential or current is implemented across the reaction cell to form nanoparticles. Integrating the electrosynthesis methods with the fast-growing nanotechnology field can present a unique gift to progress the synthesis chemistry for many applications (Mozafari and Parsa 2020; Ulyankina et al. 2020; Fani et al. 2020; Ma et al. 2021).

Molybdenum trioxide (MoO$_3$) semiconductor is highly interesting among other semiconductors because of desirable biocompatibility, high electrical conductivity, big band gape, acceptable catalytic activity, tuning plasmon, large surface area, and lower final production costs (Zhu et al. 2017; Huang et al. 2018). These superiorities facilitate the application of MoO$_3$ in several domains, such as electro-catalysis (Yang et al. 2020; Afsharpour and Dini 2019), energy storage device development (Wu et al. 2017; Dwivedi et al. 2018), and fabrication of chemical sensors (Wei et al. 2020; Samdani et al. 2017; Xue et al. 2019; Pandey et al. 2018). To this end, MoO$_3$ nanomaterials have been used

Nasrollahpour *et al. Cancer Nanotechnology*   (2023) 14:45

Page 4 of 15

in different shapes, sizes, and functionalities in biosensing strategies. One of the most prevalent interests in such an investigation is merging Mo nanostructures with other nanomaterials like platinum (Wang et al. 2016), graphene (Achadu et al. 2020), and gold (Wei et al. 2020) nanomaterials. All these combinations are proposed to boost the performance of the Mo nanostructures and cover their application gaps like poor functionality and lower conductivity compared to the noble metal nanomaterials.

In this research, we used MoO_3/poly-Tau (MoO_3/p-Tau) nanofilms as a high-performance framework for the detection of HER-2 in serum samples of BC patients. P-Tau is a conductive biopolymer that can raise the sensitivity of the biosensing framework by increasing the conductivity, enhancing the specific surface area, and effectively binding the other (nano)materials onto the electrode. In addition, taurine is considered a functional group-rich compound for nitrogen and sulfur containing groups in the structure. Considering its high biocompatibility and desirable features, combining p-Tau with other (nano)materials can be a promising tool for designing high-performance biosensors. This research applied an electrosynthesis route to fabricate the nanofilms onto the electrode for breast cancer screening. To our knowledge, this is the first report of MoO_3/p-Tau nano-films application in the bioassaying field. The highly homogeneous distribution of Mo nanoparticles into the p-Tau films was monitored using an appropriate potential range.

Experimental

Material and instruments

HER-2 antibody (Ab) and HER-2 protein were obtained from Abcam. Na_2MoO_4 powder and taurine were purchased from Merck. N-ethyl-N′-(3-(dimethylamino) propyl) carbodiimide (EDC) and N-hydroxysuccinimide (NHS) solutions were prepared in deionized water (Sigma-Aldrich). Phosphate buffer solution (PBS, pH=7.4) was prepared by dissolving 200 mg KCl, 1.44 g Na_2HPO_4, 8 g NaCl, 245 mg KH_2PO_4, in the deionized water at room temperature. Electrochemical measurements were done by using a Metrohm Autolab system and Nova software. The electrochemical system was composed of a three-electrode system, including a glassy carbon electrode (GCE) as a working electrode with 3 mm in diameter, a Pt wire as the counter electrode, and an Ag/AgCl as the reference electrode. All analyses were performed at room temperature. Before experiments, an ultrasonic bath (Model: 420; Transsonic) was applied to homogenize the solutions. The pH of solutions was controlled via a pH meter (Corning, model 120). Solutions were mixed using a magnetic stirrer,. The SEM, EDX, and dot mapping records were recorded using a Tescan instrument (Model: MIRA3).

Fabrication of the electrochemical immunosensor

Immunosensor was manufactured on a pre-cleaned 3 mm diameter GCE as the working electrode. The electrosynthesis process was performed in a three-electrode system through the cyclic voltammetry technique. All the potentials were applied versus Ag/AgCl electrode. At pH=7, the electrodeposition was switched by dipping the working electrode inside the electrochemical cell containing an aqueous solution of 5 mM Na_2MoO_4 and 0.1 M taurine. Afterward, cyclic voltammetry was carried out in the range of − 1.5 to 2.3 V with a scan rate of 0.05 V per second for 5 cycles. The modified

electrode was tagged as MoO_3/p-Tau/GCE. In the following, the modified electrodes were rinsed in deionized water. Then, a mixture of EDC/NHS/Ab (2:1:1 v/v) was prepared and after a homogenizing process, left to rest for 30 min. Antibody molecules attached to the surface via amid bound between carboxylic groups of the antibody and nitrogen groups of the poly taurine moiety of the electrodeposited film. Next, a 10 μL of the mixture was drop cast on the MoO_3/p-Tau/GCE and left for 90 min. Finally, a determined amount of HER-2 protein was incubated on the Ab-EDC-NHS/MoO_3-p-Tau/GCE for 90 min. The prepared electrode was washed with PBS solution (pH = 7.4) and analyzed with an AutoLab instrument. For comparison, other electrodes, including p-Tau/GCE and MoO_3/GCE, were fabricated using a similar approach.

HER-2 IHC staining

In this study, we performed HER-2 IHC staining to find the correlation of anaplastic changes in breast tissue with HER-2 levels in the serum of BC patients. For this purpose, patients were asked to complete the informed consent. All procedures of this study were approved by the Local Ethics Committee of Tabriz University of Medical Sciences. In BC patients, histopathological examination is touted as the gold standard for consolidated diagnosis and determination of BC anaplastic changes. The tissue fragments sampled during the surgical procedure and referred to the pathological lab were used in this study without any interference with the treatment protocol of patients. Here, we monitored the HRE-2 levels in BC samples. For IHC staining, samples were fixed in 10% formalin solution, 5 μm thick slides were prepared. Samples were incubated with 3% hydrogen peroxide solution for 20–30 min to neutralize endogenous peroxidase activity. To retrieve antigens, slides were kept in citrate buffer (pH = 6.0) for 15 min. Thereafter, an antibody targeting human HER-2 was used according to the manufacturer's instructions. After PBS washes, a secondary HRP-conjugated antibody was used. Diaminobenzidine (DAB) was used as a chromogen agent. Finally, the slides were visualized and imaged using Olympus microscopy.

Results and discussion

Clarification of the electrosynthesis methodology

To evaluate the efficiency of the protocol, the developed electrochemical biosensors were monitored using two different approaches. The cyclic voltammetry (CV) technique was used in the range of − 1.5 to 2.3 V to prepare the MoO_3/p-Tau nanofilms. According to the literature, p-Tau was electropolymerizable in positive potentials about 1.8 V vs. SCE. The electropolymerization of p-Tau was initiated by an oxidation process of a taurine molecule on its NH_2 end in positive potentials. The oxidized taurine molecule linked to a sulfur atom in another taurine molecule released an H_2O molecule to form an N-S bund between the two taurine molecules. Equation 1 depicts the whole mechanism of p-Tau formation (Hasanzadeh et al. 2014). MoO_3 was electrodeposited in the negative ranges (Yao et al. 2012; Zhao et al. 2020). In this regard, we used a potential range between − 1.5 and 2.3 V (vs. Ag/AgCl) to cover both negative and positive potentials. This feature led to the simultaneous formation of homogenous MoO_3 and p-Tau as highly ordered nanofilms. According to our data (Fig. 1A, B), two important potential points were notified on the voltammogram following the electrodeposition of
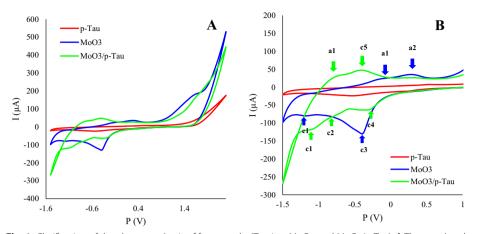
Fig. 1 Clarification of the electrosynthesis of frameworks (Taurine, MoO$_3$, and MoO$_3$/p-Tau). **A** The correlated CV voltammograms and **B** The magnified voltammograms between − 1.5 to 1 V. All the represented arrows are associated with the formation of the nano-biomaterials onto the electrode

p-Tau. The first point correlates with the oxidation of p-Tau and enhanced electropolymerization process at 1.8 V. The peak at -0.55 V would be related to the reduction of the positive p-Tau byproducts on the electrode surface. We found that both these peaks were also detectable in the CV after co-electrodeposition of MoO$_3$/p-Tau. Data showed three distinct points in the CV voltammograms of MoO$_3$/p-Tau. First, in both CV voltammograms, there are two pairs of potentials (represented as a$_1$, a$_2$, and c$_1$, c$_2$). As can be seen, the two pairs of potentials related to the MoO$_3$/p-Tau surface exhibited a sharp and reversible response compared to the electrode coated with MoO$_3$ alone, indicating a more rapid electron transferring ability of MoO$_3$/p-Tau nanofilm versus MoO$_3$ alone. The peak at about − 0.5 V on MoO$_3$/p-Tau nanofilms' growth (c$_4$) can be correlated with the reduction of p-Tau species which were produced during the anodic potentials. The cathodic peak (c$_3$) in the MoO$_3$ voltammogram is associated with the reduction of produced O$_2$ during the anodic cycle (Genies et al. 1998). This peak was not detected in MoO$_3$/p-Tau and p-Tau voltammograms. One reason would be that the reduction of O$_2$ by oxidized p-Tau species disappeared from the relevant peak.

$$nNH_2 - CH_2 - CH_2 - SO_3H \xrightarrow{Applying\,potential\,(Cyclic\,Voltammetry)}$$
$$[NH - CH_2{-}CH_2{-}SO_2 - NH{-}CH_2{-}CH_2 - SO_2]_n \qquad (1)$$

Characterization of the co-electrosynthesized MoO$_3$/p-Tau nanofilms

To confirm the electrodeposition and electrocatalytic activity of the electrosynthesized nanofilms, electrochemical and morphological characterizations were conducted. The CV and electrochemical impedance spectroscopy (EIS) techniques were implemented to prove the effectiveness of each component on the electrochemical signal's intensity. The experiments proceeded in 5 mM K$_4$[Fe(CN)$_6$] (Additional file 1: Fig. S1A, B). Noteworthy, the peak currents were increased after electropolymerization of p-Tau in comparison with bare GCE. This can be due to the increased surface area and electroconductivity of p-Tau film. According to the CV data, the signal further increased with

the co-electrosynthesis of MoO_3/p-Tau. For further confirmation, the voltammograms of electrodes coated with Molybdenum alone were studied. Data supported the fact that the peak heights of the MoO_3/p-Tau modified electrode were more than that of the MoO_3, indicating the higher conductivity of the MoO_3/p-Tau electrode. It is inferred that the combination of MoO_3 and p-Tau have a synergic and/ or structural improvement effect of increasing current compared to when used alone. The stepwise preparations and relevant data are presented in Fig. 2A, B). After incubation of electrodes with the EDC/NHS/antibody mixture, the signal intensities declined, which is linked to the steric hindrance of the EDC/NHS/antibody combination. EDC/NHS couple was used to activate the carboxylic groups of Abs. Using this strategy, the incubation time of Ab is decreased dramatically. Along with these changes, a dramatic decrease in the intensity of signals was notable after incubating the HER-2 protein. These effects can be related to the existence of antigen–antibody interaction and the gained steric repulsion of HER-2 protein.

In order to confirm the results, morphological and semiquantitative studies were performed using SEM, EDX, and dot mapping analyses (Fig. 3 and Additional file 1: S2). SEM imaging revealed that MoO_3 nanoparticles were evenly distributed inside the p-Tau matrix with a narrow particle size (about 22 nm) distribution. As can be seen from the figures visibly, the surface-to-volume ratio is the best by MoO_3/p-Tau compared to the p-Tau and MoO_3 films. The distribution quality was also confirmed by data from dot-mapping plots (Additional file 1: Fig. S2), which indicated a high-density electrode deposition of the platform o the electrode. Also, to give a clearer vision of the deposition manner of the nanofilm, we employed elemental analysis results with MoO_3/p-Tau modified electrode using EDX. According to the results (Additional file 1: Table S1), the weight percent of elements reflect the deposition quality of the proposed platform onto the electrode.

Optimization of experimental conditions

Several parameters, such as the number of deposition cycles and incubation time should be considered to boost the sensing efficiency. As a correlate, the number of deposition cycles was investigated. According to previous data, scan numbers critically impact the thickness and quality of the nanofilms. In this way, five different scan numbers, including 1, 3, 5, 8, and 10 were performed. The electrochemical readouts were increased with increasing cycle number (Additional file 1: Fig. S3A, B). This can be correlated to increasing the specific surface area as the nanofilm was grown further from 1 to 5 cycles. In cycles more than 5 cycles, the response intensity was decreased, resulting from much thickness of the nanofilms and/or decreased porosity. The incubation time of the antibody on the modified electrode surface was also optimized. Considering the time required for biorecognition and the promotion of covalent interaction on the modified electrode surface, the reduction of signal intensity is a result of the steric hindrance. By increasing the incubation time, the number of antibody molecules attached to the electrode surface is thought to be increased. As shown in Additional file 1: Fig. S4A, B), the signal intensity was decreased with an increase in the incubation time from 15 to 90 min.
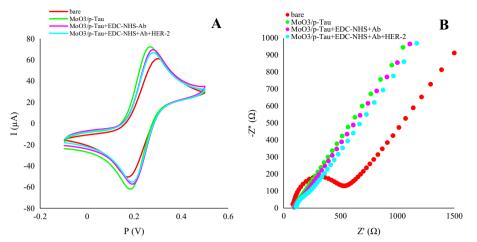
Fig. 2 Electrochemical characterization of the preparation steps of the proposed nanobiosensor. All the signals were obtained in $K_4[Fe(CN)_6]$ (5 mM)

Of note, a higher amount of time (more than 90 min) did not alter the signal readouts, which can mean the saturation of the attachment sites by Ab molecules.

Analytical performance characteristics

Quantitative recognition of the target protein was tried out under the optimized conditions by incubating six different concentrations of HER-2 protein (0.1, 0.01, 0.001, 0.0001, 0.00001, and 0.000001 ng/mL) with the designed transducer. As illustrated in Fig. 4A, B), the electrochemical response was orderly decreased upon the increased HER-2 concentration. The data represents a good linear correlation between the signal intensity and related concentrations ($r^2 = 99.78$). We found a lower limit of quantification (LLOQ) at the range of 1 fg/mL. These data demonstrated the suitability of the developed immunosensor for the analysis of HER-2 protein at the femtogram levels. The specificity of the biosensor was evaluated. In this regard, we assessed the effect of three possible interferences (CEA, CA-15-3, and BSA proteins) on the electrochemical readouts (Additional file 1: Fig. S5A, B). The one-by-one interfering effects and also the cumulative effect of them were checked. Also, the 10 and 100 folds of interferences concentrations were applied in cumulative format for better comparison. Based on the recorded results, the mentioned proteins have little effect on the signals. Additionally, the prepared bioassay was successfully checked in normal serum samples by spiking the target HER-2 protein.

To evaluate the effect of electrode type on the recorded responses, three different electrodes were modified by the same procedure, and the electrochemical response was gained for 0.01 pg/mL of HER-2. Again, signals displayed a practicable reproducibility using our protocol (Additional file 1: Fig. S6A, B). The stability of signals was also assessed by the fabrication of electrodes under the optimized conditions and by recording ten repetitive DPV signals exposed to 1 fg/mL HER-2. Data showed an RSD of 0.51% (Additional file 1: Fig. S7A, B) and Table 1).

The performance of biosensors can be compared together from several domains. First, the employed (nano) materials and implemented synthetic protocols should be attended.
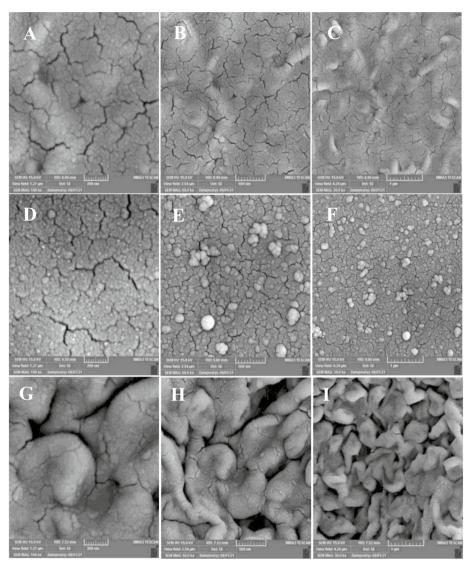
Fig. 3 The SEM images of three different modified electrodes at different magnitudes of 200, 500 and 1000 nm. **A–C** The electrode modified with electrosynthesized MoO_3 nanoparticles. **D–F**) The electrode modified with electrografted p-Tau nano-scaffolds. **G–I** The electrode modified with electrosynthesized MoO_3/p-Taunanofilms

It is highly significant that the synthesis strategies and the materials in the framework's constructions be biocompatible, environmentally friendly, eco-friendly and easy to prepare. The second option is the analytical performance, such as sensitivity, selectivity, stability, and repeatability, which should have as high as possible. As shown in Table 1 the summarized details regarding other investigations can help us develop further analyses. There are some tips that can be considered from the current experiments. First, our synthesis methodology is an electrosynthesis procedure that correlates with low reagent consumption and high preparation rate, making the protocol more biocompatible and environmentally friendly. The latter point is that we used biocompatible materials to construct the sensing platform. MoO_3 is a cheap and biocompatible compound that makes a desirable combination with p-Tau biopolymer for biosensing purposes. The
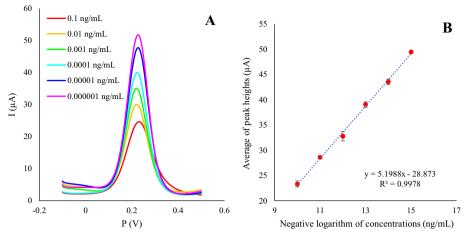
Fig. 4 **A** HER-2 bioassaying by application of DPV between 0.1–0.000001 ng/mL, **B** calibration curve of minus logarithm of HER-2 concentration (ng/mL) vs average current (µA) (n = 3)

Table 1 Comparison of the analytical features with other biosensors for HER-2 protein

Applied nanomaterial	Methode	Synthesis mechanism	Synthesis time of nanomaterials (min)	LOD	LDR	Ref.
GCE	Sandwich typed label assited	GO/PDA-FC-Au@Ag NSs[a] Ni@PtNi HNCs[b]	Wet chemical method	0.01–100 ng/mL	3.3 pg/mL	Wang et al. 2021a)
SPCE	Sandwich typed- Label free	CeO$_2$/PEG[c]	Wet chemical method	0.001–0.5 ng/ML and 0.5–20.0 ng/mL	34.9 pg/mL	Hartati et al. 2020)
GCE	Direct-Label free	Fe3O4@ TMU-21[d] MWCNTs[e]	Wet chemical method	1 pg/mL-100 ng/mL	0.3 pg/mL	Ehzari et al. 2020)
Au SPE	Direct-label free	Phenol MIP[f]	Electropolymerization	10–70 ng/mL	5.2 ng/mL	Pacheco et al. 2018)
GCE	Direct-label free	PEDOT[g]	Electrosynthesis	0.1 ng/mL-1 µg/mL	45 pg/mL	Wang et al. 2021b)
GCE	Direct-label free	MoO$_3$/p-Tau	Electrosynthesis	0.1 ng/mL-1 pg/mL	1 fg/mL	This work

[a] Graphene oxide-polydopamine-grafted-ferrocene/Au@Ag nanoshuttles

[b] Hollow Ni@PtNi yolk-shell nanocages-thionine

[c] Cerium oxide/polyethylene glycol

[d] Metal-organic framework

[e] Multi-walled carbon nanotubes

[f] Molecularly imprinted polymer

[g] Poly(3,4-ethylene dioxythiophene)

obtained lower limit of quantification (LLOQ) of the present study offers a more sensitive strategy for immunosensing of HER-2 in serum levels compared to other available approaches.
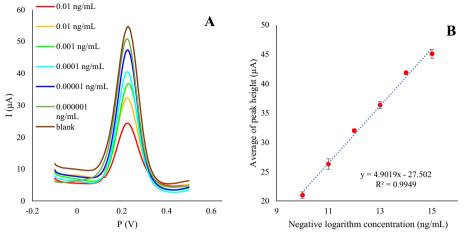
Fig. 5 Biosensing of HER-2 via standard addition methodology of determined amount of the protein (0.1–0.000001 ng/mL) in untreated serum samples. **A** DPV curves and **B** the correlated histograms (n = 3)

Real sample analysis

A calibration curve was plotted using the standard addition method to obtain a more reliable and accurate analysis. This way, six different concentrations of HER-2, including 0.1, 0.01, 0.001, 0.0001, 0.00001, and 0.000001 ng/mL, were prepared in the independent serum samples of a healthy individual (Fig. 5A, B). In comparison to Fig. 4, similar responses were recorded according to Fig. 5 but with decreased signals. This is correlated to the matrix effect of the real untreated samples. 6 (A and B) is illustrated the obtained signal readouts for four HER-2 positive volunteer patients.

Pathological studies

Histopathological examination revealed the existence of HER-2$^+$ cells inside the breast tissues with malignancies. The intensity of HER-2 and the number of HER-2$^+$ cells were different in different samples enrolled in this study. The uncontrolled increase of HER-2 correlates with aggressive histological remodeling and poor diagnosis in BC patients. We noted numerous infiltrating carcinoma cells into the mammary gland tissue, forming aggregates. These cells were positive to a membrane tyrosine kinase, namely HER-2, showing malignancy. However, the intensity and number of HER-2$^+$ varied in samples of different BC patients. These data showed that in HER-2 positive BC, ductal cells could express large levels of this factor that varies between the samples. The pathological images are presented in Fig. 6C.

Conclusions

This research successfully constructed a high-performance and ultrasensitive electrochemical immunoassay for BC analysis based on a biocompatible and environmentally friendly MoO$_3$/p-Tau nanofilm. The nanostructure was fabricated onto the electrode through the electrosynthesis approach as an environmentally and eco-friendly synthesis route. It is suggested that p-Tau can be employed for two purposes: I) increasing the specific surface area for attachment of MoO$_3$ and antibody molecules; II) providing a
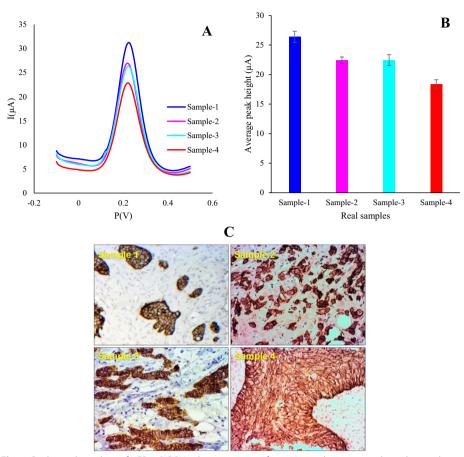
Fig. 6 Real sample analysis of HER-2 **A** DPV voltammograms of unprocessed serum sample analysis with developed bioassay, **B** Corresponded histograms and **C** correlated phatological images (samples 1, 2, 3 and 4) (n = 3)

highly stable substrate to hold MoO_3 nanoparticles from releasing during the measurements. Besides, MoO_3 was utilized to enhance the conductivity, boosting the signal intensity. The designed nano-immunoassay displayed a desirable LLOQ of 1 fg/mL with a wide dynamic range of 0.1 ng/mL to 1 fg/mL. We implemented two calibration plots (in standard solutions and healthy blank serum) to give more insights and prove the proposed nanobiosensor's reliability. Also, to establish the applicability of the proposed framework, it was tested for the analysis of HER-2 positive real samples. Interestingly, the obtained results were confirmed by pathological studies. The results indicated an excellent ability for the biosensor in diagnosing breast cancer.

Supplementary Information

The online version contains supplementary material available at https://doi.org/10.1186/s12645-023-00201-x.

Additional file 1: Figure S1. Investigation of the effect of each modifier on the electrochemical behavior of the proposed framework. All the data were obtained in $K_4[Fe (CN)_6]$ (5 mM). **Figure S2.** The EDX and dot mapping quantitative elemental analysis of the different modified electrodes. **A** and **B**: MoO_3 modified electrode. **C** and **D**: p-Tau modified electrode. E and F: MoO3/p-Tau modified electrode. **Figure S3.** Effect of the deposition cycle numbers on the electrochemical signals. **A** DPV voltammograms and **B** Correlated histograms. All the signals were obtained in $K_4[Fe(CN)_6]$ (5 mM). **Figure S4.** Incubation time study of anti-HER-2 on the as-prepared MoO3/p-Tau/GCE at different time points (10, 30, 45, 60, 90, and 120 min). **Figure S5.** Evaluation of the selectivity of the design immunosensor in

the presence of 10 pg/mL of CEA, BSA, and CA-15-3, different concentrations of HER-2 (1pg/mL and 1 fg/mL) and also in the presence of a mixture of them. **Figure S6.** The reproducibility screening of the suggested framework at three different electrodes with the same procedure. **Figure S7.** The signal stability of the immunosensor for 10 consecutive signals. **Table S1.** The elemental analysis results with MoO_3/p-Tau modified electrode using Energy Dispersive X-Ray Analysis (EDX).

Availability of data and materials
Not applicable.

Declarations

Ethics approval and consent to participate
Ethics approval and consent to participate All patients were asked to complete the informed consent. All procedures of this study were approved by the Local Ethics Committee of Tabriz University of Medical Sciences (IR.TBZMED.VCR.REC.1400.150). All procedures were done under the declaration of Helsinki.

Consent for publication
Not applicable.

Competing interests
The authors declare no competing interests.

References
Achadu OJ, Abe F, Suzuki T, Park EY (2020) Molybdenum trioxide nanocubes aligned on a graphene oxide substrate for the detection of norovirus by surface-enhanced raman scattering. ACS Appl Mater Interfaces 12(39):43522–43534. https://doi.org/10.1021/acsami.0c14729

Afsharpour M, Dini Z (2019) One-pot functionalization of carbon nanotubes by WO3/MoO3 nanoparticles as oxidative desulfurization catalysts. Fullere Nanotub Carbon Nanostruct 27(3):198–205. https://doi.org/10.1080/1536383X.2018.1538132

Ansari SA, Khan NA, Hasan Z, Shaikh A, Ferdousi FK, Barai HR, Lopa NS, Rahman MM (2020) Electrochemical synthesis of titanium nitride nanoparticles onto titanium foil for electrochemical supercapacitors with ultrafast charge/discharge. Sustain Energy Fuels 4(5):2480–2490. https://doi.org/10.1039/D0SE00049C

Cesewski E, Johnson BN (2020) Electrochemical biosensors for pathogen detection. Biosens Bioelectron. https://doi.org/10.1016/j.bios.2020.112214

Chen Y, Fan Z, Zhang Z, Niu W, Li C, Yang N, Chen B, Zhang H (2018) Two-dimensional metal nanomaterials: synthesis, properties, and applications. Chem Rev 118(13):6409–6455. https://doi.org/10.1021/acs.chemrev.7b00727

Chen D, Wang D, Hu X, Long G, Zhang Y, Zhou L (2019) A DNA nanostructured biosensor for electrochemical analysis of HER2 using bioconjugate of GNR@Pd SSs—Apt—HRP. Sensors Actuators B Chem. https://doi.org/10.1016/j.snb.2019.126650

Chenaghlou S, Khataee A, Jalili R, Rashidi M-R, Khalilzadeh B, Joo SW (2021) Gold nanostar-enhanced electrochemiluminescence immunosensor for highly sensitive detection of cancer stem cells using CD133 membrane biomarker. Bioelectrochemistry 137:107633. https://doi.org/10.1016/j.bioelechem.2020.107633

Chun L, Kim S-E, Cho M, Choe W-s, Nam J, Lee DW, Lee Y (2013) Electrochemical detection of HER2 using single stranded DNA aptamer modified gold nanoparticles electrode. Sensors Actuators Chem 186:446–450. https://doi.org/10.1016/j.snb.2013.06.046

Dwivedi C, Mohammad T, Bharti V, Patra A, Pathak S, Dutta V (2018) CoSP approach for the synthesis of blue MoO3 nanoparticles for application as hole transport layer (HTL) in organic solar cells. Sol Energy 162:78–83. https://doi.org/10.1016/j.solener.2017.12.063

Ehzari H, Samimi M, Safari M, Gholivand MB (2020) Label-free electrochemical immunosensor for sensitive HER2 biomarker detection using the core-shell magnetic metal-organic frameworks. J Electroanal Chem. https://doi.org/10.1016/j.jelechem.2020.114722

Fani M, Rezayi M, Pourianfar HR, Meshkat Z, Makvandi M, Gholami M, Rezaee SA (2020) Rapid and label-free electrochemical DNA biosensor based on a facile one-step electrochemical synthesis of rGO–PPy–(l-Cys)–AuNPs nanocomposite for the HTLV-1 oligonucleotide detection. Biotechnol Appl Biochem. https://doi.org/10.1002/bab.1973

Genies L, Faure R, Durand R (1998) Electrochemical reduction of oxygen on platinum nanoparticles in alkaline media. Electrochim Acta 44(8–9):1317–1327. https://doi.org/10.1016/S0013-4686(98)00254-0

Gupta R, Raza N, Bhardwaj SK, Vikrant K, Kim K-H, Bhardwaj N (2021) Advances in nanomaterial-based electrochemical biosensors for the detection of microbial toxins, pathogenic bacteria in food matrices. J Hazard Mater 401:123379. https://doi.org/10.1016/j.jhazmat.2020.123379

Hartati YW, Letelay LK, Gaffar S, Wyantuti S, Bahti HH (2020) Cerium oxide-monoclonal antibody bioconjugate for electrochemical immunosensing of HER2 as a breast cancer biomarker. Sens Bio-Sens Res 27:100316. https://doi.org/10.1016/j.sbsr.2019.100316

Hasanzadeh M, Pournaghi-Azar MH, Shadjou N, Jouyban A (2014) Electropolymerization of taurine on gold surface and its sensory application for determination of captopril in undiluted human serum. Mater Sci Eng C 38:197–205. https://doi.org/10.1016/j.msec.2014.01.051

Huang W, Zhou Y, Du J, Deng Y, He Y (2018) Versatile visual logic operations based on plasmonic switching in label-free molybdenum oxide nanomaterials. Anal Chem 90(3):2384–2388. https://doi.org/10.1021/acs.analchem.7b05097

Isildak I, Navaeipour F, Afsharan H, Kanberoglu GS, Agir I, Ozer T, Annabi N, Totu EE, Khalilzadeh B (2020) Electrochemiluminescence methods using CdS quantum dots in aptamer-based thrombin biosensors: a comparative study. Microchim Acta 187(1):1–13. https://doi.org/10.1007/s00604-019-3882-y

Karimzadeh Z, Hasanzadeh M, Isildak I, Khalilzadeh B (2020) Multiplex bioassaying of cancer proteins and biomacromolecules: Nanotechnological, structural and technical perspectives. Int J Biol Macromol 165:3020–3039. https://doi.org/10.1016/j.ijbiomac.2020.10.191

Khalilzadeh B, Rashidi M, Soleimanian A, Tajalli H, Kanberoglu GS, Baradaran B, Rashidi M-R (2019) Development of a reliable microRNA based electrochemical genosensor for monitoring of miR-146a, as key regulatory agent of neurodegenerative disease. Int J Biol Macromol 134:695–703. https://doi.org/10.1016/j.ijbiomac.2019.05.061

Kim S, Kim TG, Lee SH, Kim W, Bang A, Moon SW, Song J, Shin JH, Yu JS, Choi S (2020) Label-Free surface-enhanced raman spectroscopy biosensor for on-site breast cancer detection using human tears. ACS Appl Mater Interfaces 12(7):7897–7904. https://doi.org/10.1021/acsami.9b19421

Kolahalam LA, Viswanath IK, Diwakar BS, Govindh B, Reddy V, Murthy Y (2019) Review on nanomaterials: synthesis and applications. Mater Today Proc 18:2182–2190. https://doi.org/10.1016/j.matpr.2019.07.371

Loyez M, Hassan EM, Lobry M, Liu F, Caucheteur C, Wattiez R, DeRosa MC, Willmore WG, Albert J (2020) Rapid detection of circulating breast cancer cells using a multiresonant optical fiber aptasensor with plasmonic amplification. ACS Sens 5(2):454–463. https://doi.org/10.1021/acssensors.9b02155

Ma Y, Zhang Y, Wang L (2021) An electrochemical sensor based on the modification of platinum nanoparticles and ZIF-8 membrane for the detection of ascorbic acid. Talanta. https://doi.org/10.1016/j.talanta.2021.122105

Mansouri M, Khalilzadeh B, Barzegari A, Shoeibi S, Isildak S, Bargahi N, Omidi Y, Dastmalchi S, Rashidi M-R (2020) Design a highly specific sequence for electrochemical evaluation of meat adulteration in cooked sausages. Biosens Bioelectron 150:111916. https://doi.org/10.1016/j.bios.2019.111916

Min J, Sempionatto JR, Teymourian H, Wang J, Gao W (2021) Wearable electrochemical biosensors in North America. Biosens Bioelectron 172:112750. https://doi.org/10.1016/j.bios.2020.112750

Mozafari V, Parsa JB (2020) Electrochemical synthesis of Pd supported on PANI-MWCNTs-SnO2 nanocomposite as a novel catalyst towards ethanol oxidation in alkaline media. Synthetic Metals 259:116214. https://doi.org/10.1016/j.synthmet.2019.116214

Nasrollahpour H, Isildak I, Rashidi M-R, Hashemi EA, Naseri A, Khalilzadeh B (2021a) Ultrasensitive bioassaying of HER-2 protein for diagnosis of breast cancer using reduced graphene oxide/chitosan as nanobiocompatible platform. Cancer Nanotechnol 12(1):1–16. https://doi.org/10.1186/s12645-021-00082-y

Nasrollahpour H, Mahdipour M, Isildak I, Rashidi M-R, Naseri A, Khalilzadeh B (2021) A highly sensitive electrochemiluminescence cytosensor for detection of SKBR-3 cells as metastatic breast cancer cell line: a constructive phase in early and precise diagnosis. Biosensors Bioelectron. https://doi.org/10.1016/j.bios.2021.113023

Pacheco JG, Rebelo P, Freitas M, Nouws HPA, Delerue-Matos C (2018) Breast cancer biomarker (HER2-ECD) detection using a molecularly imprinted electrochemical sensor. Sens Actuators B Chem 273:1008–1014. https://doi.org/10.1016/j.snb.2018.06.113

Pandey S, Sharma AK, Sharma KH, Nerthigan Y, Khan MS, Hang D-R, Wu H-F (2018) Rapid naked eye detection of alkaline phosphatase using α-MoO3-x nano-flakes. Sens Actuators b Chem 254:514–518. https://doi.org/10.1016/j.snb.2017.06.123

Pourakbari R, Shadjou N, Yousefi H, Isildak I, Yousefi M, Rashidi M-R, Khalilzadeh B (2019) Recent progress in nanomaterial-based electrochemical biosensors for pathogenic bacteria. Microchim Acta 186(12):1–13. https://doi.org/10.1007/s00604-019-3966-8

Ranganathan V, Srinivasan S, Singh A, DeRosa MC (2020) An aptamer-based colorimetric lateral flow assay for the detection of human epidermal growth factor receptor 2 (HER2). Anal Biochem 588:113471. https://doi.org/10.1016/j.ab.2019.113471

Samdani KJ, Joh DW, Rath MK, Lee KT (2017) Electrochemical mediatorless detection of norepinephrine based on MoO3 nanowires. Electrochim Acta 252:268–274. https://doi.org/10.1016/j.electacta.2017.08.187

Sharma S, Zapatero-Rodriguez J, Saxena R, O'Kennedy R, Srivastava S (2018) Ultrasensitive direct impedimetric immunosensor for detection of serum HER2. Biosens Bioelectron 106:78–85. https://doi.org/10.1016/j.bios.2018.01.056

Shen C, Liu S, Li X, Zhao D, Yang M (2018) Immunoelectrochemical detection of the human epidermal growth factor receptor 2 (HER2) via gold nanoparticle-based rolling circle amplification. Mikrochim Acta 185(12):547. https://doi.org/10.1007/s00604-018-3086-x

Tabasi A, Noorbakhsh A, Sharifi E (2017) Reduced graphene oxide-chitosan-aptamer interface as new platform for ultrasensitive detection of human epidermal growth factor receptor 2. Biosens Bioelectron 95:117–123. https://doi.org/10.1016/j.bios.2017.04.020

Ulyankina A, Molodtsova T, Gorshenkov M, Leontyev I, Zhigunov D, Konstantinova E, Lastovina T, Tolasz J, Henych J, Licciardello N (2020) Photocatalytic degradation of ciprofloxacin in water at nano-ZnO prepared by pulse alternating current electrochemical synthesis. J Water Process Eng. https://doi.org/10.1016/j.jwpe.2020.101809

Wang A-L, Liang C-L, Lu X-F, Tong Y-X, Li G-R (2016) Pt–MoO 3–RGO ternary hybrid hollow nanorod arrays as high-performance catalysts for methanol electrooxidation. J Mater Chem A 4(5):1923–1930. https://doi.org/10.1039/C5TA08585C

Wang Y-H, Huang K-J, Wu X (2017) Recent advances in transition-metal dichalcogenides based electrochemical biosensors: a review. Biosensors Bioelectronics 97:305–316. https://doi.org/10.1016/j.bios.2017.06.011

Wang H, Zhao W, Zhao Y, Xu C-H, Xu J-J, Chen H-Y (2020) Real-time tracking the electrochemical synthesis of Au@ metal core-shell nanoparticles toward photo enhanced methanol oxidation. Anal Chem 92(20):14006–14011. https://doi.org/10.1021/acs.analchem.0c02913

Wang X-Y, Feng Y-G, Wang A-J, Mei L-P, Yuan P-X, Luo X, Feng J-J (2021) A facile ratiometric electrochemical strategy for ultrasensitive monitoring HER2 using polydopamine-grafted-ferrocene/reduced graphene oxide, Au@ Ag nanoshuttles and hollow Ni@ PtNi yolk-shell nanocages. Sens Actuators B Chem 331:129460. https://doi.org/10.1016/j.snb.2021.129460

Wang W, Han R, Chen M, Luo X (2021b) Antifouling peptide hydrogel based electrochemical biosensors for highly sensitive detection of cancer biomarker HER2 in human serum. Anal Chem 93(19):7355–7361. https://doi.org/10.1021/acs.analchem.1c01350

Wei C, Cen M, Chui H-C, Cao T (2020) Numerical study of biosensor based on α-MoO3/Au hyperbolic metamaterial at visible frequencies. J Phys D: Appl Phys 54(3):034001. https://doi.org/10.1088/1361-6463/abbb08/meta

Wongkaew N, Simsek M, Griesche C, Baeumner AJ (2018) Functional nanomaterials and nanostructures enhancing electrochemical biosensors and lab-on-a-chip performances: recent progress, applications, and future perspective. Chem Rev 119(1):120–194. https://doi.org/10.1021/acs.chemrev.8b00172

Wu Z, Lei W, Wang J, Liu R, Xia K, Xuan C, Wang D (2017) Various structured molybdenum-based nanomaterials as advanced anode materials for lithium ion batteries. ACS Appl Mater Interfaces 9(14):12366–12372. https://doi.org/10.1021/acsami.6b16251

Xue J, Yang L, Jia Y, Zhang Y, Wu D, Ma H, Hu L, Wei Q, Ju H (2019) Dual-quenching electrochemiluminescence resonance energy transfer system from Ru–In2S3 to α-MoO3-Au based on protect of protein bioactivity for procalcitonin detection. Biosens Bioelectron 142:111524. https://doi.org/10.1016/j.bios.2019.111524

Yang G, Yang H, Zhang X, Feng F, Ma J, Qin J, Yuan F, Cai Y, Ma J (2020) Surfactant-free self-assembly to the synthesis of MoO3 nanoparticles on mesoporous SiO2 to form MoO3/SiO2 nanosphere networks with excellent oxidative desulfurization catalytic performance. J Hazard Mater 397:122654. https://doi.org/10.1016/j.jhazmat.2020.122654

Yao DD, Ou JZ, Latham K, Zhuiykov S, O'Mullane AP, Kalantar-zadeh K (2012) Electrodeposited α-and β-phase MoO3 films and investigation of their gasochromic properties. Crystal Growth Design 12(4):1865–1870. https://doi.org/10.1021/cg201500b

Zhang Y, Chen X (2019) Nanotechnology and nanomaterial-based no-wash electrochemical biosensors: from design to application. Nanoscale 11(41):19105–19118. https://doi.org/10.1039/C9NR05696C

Zhang Z, Feng C, Liu C, Zuo M, Qin L, Yan X, Xing Y, Li H, Si R, Zhou S (2020) Electrochemical deposition as a universal route for fabricating single-atom catalysts. Nat Commun 11(1):1–8. https://doi.org/10.1038/s41467-020-14917-6

Zhao N, Fan H, Zhang M, Ma J, Du Z, Yan B, Li H, Jiang X (2020) Simple electrodeposition of MoO3 film on carbon cloth for high-performance aqueous symmetric supercapacitors. Chem Eng J 390:124477. https://doi.org/10.1016/j.cej.2020.124477

Zhu Y, Chen G, Xu X, Yang G, Liu M, Shao Z (2017) Enhancing electrocatalytic activity for hydrogen evolution by strongly coupled molybdenum nitride@ nitrogen-doped carbon porous nano-octahedrons. ACS Catal 7(5):3540–3547. https://doi.org/10.1021/acscatal.7b00120

Publisher's Note

Springer Nature remains neutral with regard to jurisdictional claims in published maps and institutional affiliations.